

DOI: 10.13208/j.electrochem.1511152

Artical ID:1006-3471(2016)02-0101-12

Cite this: *J. Electrochem.* 2016, 22(2): 101-112

Http://electrochem.xmu.edu.cn

# 包覆型非贵金属氧还原催化剂的研究进展

肖梅玲<sup>1,2</sup>, 祝建兵<sup>1,2</sup>, 刘长鹏<sup>2</sup>, 葛君杰<sup>2</sup>, 邢 巍<sup>1,2\*</sup>

(1. 中国科学院长春应用化学研究所, 电分析国家重点实验室, 吉林 长春 130022;  
2. 中国科学院长春应用化学研究所, 先进化学电源实验室, 吉林 长春 130022)

**摘要:** 燃料电池中广泛使用的铂基催化剂价格昂贵、储量低、容易失活, 因此亟待开发廉价、高效非铂催化剂。过渡金属(Fe、Co、Ni 等)/杂原子共掺杂催化剂、杂原子掺杂(N、P、S、F 等)碳材料以及碳材料包覆过渡金属复合物是目前发现的几类性能优异的非贵金属氧还原催化剂。其中碳材料包覆过渡金属催化剂作为一类新型的高性能催化剂, 对其研究还有待深入。本文主要阐述了国内外在包覆型非贵金属氧还原催化剂方面的研究进展, 从合成、性能、机理等方面对该类催化剂进行了总结, 力求助益于该类催化剂的发展。

**关键词:** 氧还原反应; 过渡金属包覆; 非贵金属催化剂

**中图分类号:** O646

**文献标识码:** A

对于一些能量转化与存储装置, 如燃料电池/金属-空气电池, 氧气的还原成为影响这些装置性能的关键步骤。目前, 最好的氧还原催化剂仍主要采用 Pt/C 催化剂, 然而 Pt 价格昂贵, 储量低, 易中毒失活。因此, 开发廉价、高效、稳定的非铂基阴极氧还原催化剂成为了研究热点。在 1964 年, Jansink<sup>[1]</sup>在 *Nature* 杂志上发表了钴酞菁大环化合物在碱性介质中催化氧还原反应的论文。随后, 许多种不同结构的大环配合物被证实具有催化氧还原反应的活性<sup>[2-12]</sup>。其中, 以过渡金属 Fe、Co 为中心的大环配合物具有更高的活性<sup>[13-14]</sup>。对于这种大环配合物, 研究人员发现它们在酸性介质中的稳定性较差, 活性也有待提高, 而在惰性气体氛围中热处理后, 催化剂的活性和稳定性得到了提高<sup>[15-18]</sup>。但大环配合物的合成比较复杂, 研究人员尝试采用金属无机物作为金属源、含氮的小分子作为氮前驱体和碳载体一起进行热处理, 所得产物也有可观的催化活性和稳定性。在此之后, 各种不同的前驱体源组合被用来合成这类催化剂, 如 2009 年 Dodellet 教授研究组<sup>[19]</sup>报道了利用聚苯胺为氮源、金属无机盐为金属前驱体与碳黑一起热处理得到这

种类型的催化剂, 活性和稳定性已经接近了美国能源部设定的 2015 年研究目标。目前, 这类催化剂的研究重点和难点是活性位点的探究<sup>[20-24]</sup>。此外, 非金属杂原子掺杂碳材料也被报道具有催化氧还原性能, 如氮掺杂碳、硫掺杂碳、磷掺杂碳、氟掺杂碳及其二元或三元杂原子共掺杂<sup>[25-29]</sup>。这类非金属碳基催化剂在碱性介质中的性能已经与 Pt 相当, 但在酸性介质中催化性能与 Pt/C 催化剂相比仍有很大差距。近年来, 一类新型的碳层包覆类非贵金属催化剂逐渐引起了研究者的关注<sup>[30-35]</sup>。这类催化剂的结构主要为 1~8 层石墨化层包覆的过渡金属或者其过渡金属碳化物纳米粒子。由于过渡金属被包覆在石墨层中, 这种包覆型催化剂的稳定性有了极大的提高。这种结构的表面是碳层, 而单纯的碳层并不具备良好的氧还原催化性能, 对这种不同常规的催化剂的理解为非贵金属氧还原催化剂的研究提供了一种新的思路和方向。本文将结合作者课题组近年取得的初步研究成果, 简述这种包覆型催化剂的研究进展, 并展望今后非铂氧还原催化剂的研究方向。

## 1 包覆型催化剂的合成

收稿日期: 2016-01-05, 修订日期: 2016-03-11 \* 通讯作者, Tel: (86-437)85262223, E-mail: xingwei@ciac.ac.cn

科技部 973 项目(No. 2012CB215500)、国家自然科学基金项目(No. 21373199, No. 21433003)、中国科学院先导专项(No. XDA09030104)、吉林省科技发展项目(No. 20130206068GX, No. 20140203012SF, No. 20102204)和吉林省自然科学基金项目(No. 20150101066JC)资助

过渡金属包覆型催化剂最早用于催化氧还原反应见于 2012 年中科院大连化物所包信和院士报导<sup>[36]</sup>. 在随后几年内, 对此类催化剂研究增加并陆续开发出不同的制备方法, 归纳起来包覆型催化剂的合成方法主要可分为四类. 第一类: 先合成包覆过渡金属后热解的方法. Müllen 等<sup>[37]</sup>在水热条件下先合成碳氮包覆的  $\text{Fe}_3\text{O}_4$  粒子, 然后热解得到了氮掺杂三维石墨稀包覆  $\text{Fe}_3\text{O}_4$  纳米粒子催化剂. 第二类: 采用过渡金属原位催化方法合成过渡金属包覆型催化剂. Zhu 等<sup>[34]</sup>直接以二氰二胺、氯化铁、氧化碳黑为前驱体, 高温热解得到了氮掺杂碳纳米管包覆碳化铁催化剂, 通过对前驱体碳材料表面改性, 发现碳材料表面的含氧基团对形成这种包覆型结构起着不可或缺的作用. Xiao 等<sup>[33]</sup>将氯化铁氧化聚合后的苯二胺直接热解合成了包覆碳化铁的、具有大孔/介孔分级孔结构的三维碳材料. 第三类: 采用气相沉积方法制备. Fan 和 Flahaut 等<sup>[38-39]</sup>报导了气相沉积法制备了一系列的石墨稀纳米带包覆过渡金属碳化物 ( $\text{Fe}_3\text{C}$ 、 $\text{Co}_3\text{C}$  和  $\text{Ni}_3\text{C}$ ) 纳米阵列催化剂. 通过溅射的方法先将过渡金属沉积到基底材料表面, 在甲烷、氢气气氛下沉积得到目标催化剂, 如图 1 所示. Cui 等<sup>[40]</sup>将过渡金属先沉积到 SBA-15 模板中, 然后通过气相沉积法合成了一系列碳纳米管联结的单层石墨稀包覆过渡金属的催化剂. 第四类: 高温高压合成. 在密闭反应釜中高温高压条件下, 含过渡金属有机物分解形成包覆结构的催化剂. Deng 等<sup>[36]</sup>以二茂铁、叠氮化钠为原料氮气保护  $350^\circ\text{C}$  条件下合成了豆荚状碳纳米管包覆  $\text{FeO}_x$  催化剂. Hu 等<sup>[32, 41]</sup>以二茂铁、单氰胺为前驱体在高压反应釜中  $700^\circ\text{C}$  反应得到了石墨化碳层包覆碳化铁粒子空心球催化剂, 进一步通过改变反应温度得到了氮掺杂碳包覆  $\text{Fe}_3\text{C}$  粒子/石墨烯催化剂.

## 2 催化剂性能评价

由于催化剂制备过程中所采用的合成方法、实验条件不尽相同, 同时非贵金属催化剂具有组成、结构的复杂性, 想完美地比较不同催化剂的催化氧还原活性比较困难. 目前, 对非贵金属氧还原催化剂比较严谨的评价方法主要为比较如下几个参数: 1) 催化剂的翻转频率, 即在给定的电位和条件下每个催化位点每秒的电子转移数. 2) 催化剂的体积比活性, 即每立方厘米活性位点数. 对于铂基氧还原催化剂, 不同催化剂的性能可通过在 0.9

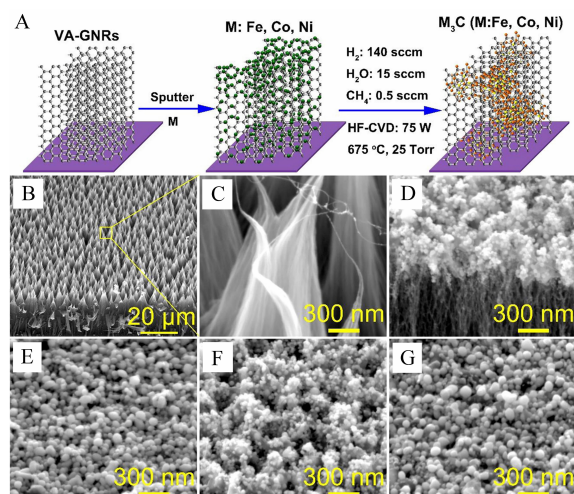


图 1 A. 在碳纳米管阵列上生长碳层包覆过渡金属碳化物的示意图; B-C. 圆锥状碳纳米管阵列的扫描电镜图; D. 所制备的碳层包覆过渡金属碳化物-碳纳米管阵列的扫描电镜照片; E-G 碳纳米管阵列顶端生长的过渡金属碳化物扫描电镜照片<sup>[38-39]</sup>

Fig. 1 A. Schematic illustration for the formation mechanism of nanocrystalline  $\text{M}_3\text{C}$  (M: Fe, Co, Ni) on VA-GNRs; B-C. SEM images of VA-GNRs with "teepee" structure; D. Typical SEM image of  $\text{M}_3\text{C}$ -GNRs; E-G. SEM images of  $\text{M}_3\text{C}$  (M: Fe, Co, Ni) NCs grown on the tips of VA-GNRs<sup>[38-39]</sup>

V vs. RHE 电位下催化剂的活性进行比较. 然而对于大多数非贵金属催化剂而言, 在该电位下催化剂几乎未表现出明显的催化氧还原活性, 因此一些课题组选取其他电位下, 如 0.5/0.7 或 0.8 V vs. RHE, 对催化剂性能进行比较, 对比较电位选取的准则是尽量避免传质效应影响. 事实上, 由于催化剂的氧还原性能是根据测定不同转速下的电流-电压极化曲线得到的, 因此, 根据 Koutecky-Levich 计算方程得到的动力学电流被广泛地用于比较不同催化剂的催化性能. 3) 通过比较不同催化剂的氧气还原过程中的电子转移数和过氧化氢产率来比较催化剂的性能. 特别是针对当前主流的非贵金属氧还原催化剂-碳基催化剂, 由于碳催化剂的稳定性深受反应过程中过氧化氢根等的影响, 因此考察该类催化剂氧还原过程中的电子转移数和双氧水产率也是评价催化剂催化性能的重要指标. 对新兴的包覆型非贵金属氧还原催化剂, 由于在保证碳层对过渡金属的完全包覆的同时其内部的金属粒子尺寸尽可能小, 外部碳层尽可能少<sup>[41]</sup>, 因此, 在催化剂的合成过程中需要采用特殊的合成

方法或处理手段导致了该类催化剂难以大批量合成、催化剂在电池中应用的工艺条件还不够成熟等问题。目前,对该类型的催化剂的评价方式主要还是通过比较催化剂的起始还原电位/半波电位或特定电位下的动力学电流密度来实现。在此,作者主要通过这两个参数来对目前报导的包覆型非贵金属氧还原催化剂在酸性和碱性条件下的催化性能分别做一个总结。

## 2.1 酸性条件下包覆型非贵金属氧还原催化剂性能

现阶段,酸性条件下包覆型非贵金属氧还原催化剂的报导较少,主要集中在包信和课题组和作者课题组。关于此类催化剂酸性条件下应用于氧还原的报导最早见于包信和课题组<sup>[36]</sup>,2012年,他们报导合成了一系列的豆荚状碳纳米管包覆过渡金属纳米粒子的包覆型氧还原催化剂(Pod(N)-Fe、Pod(N)-FeCo)。在氧气饱和的  $0.1 \text{ mol} \cdot \text{L}^{-1} \text{H}_2\text{SO}_4$  电解液中,其最好的催化剂 Pod(N)-FeCo 催化氧还原的起始电位达到  $0.6 \text{ V vs RHE}$  左右,在  $\text{H}_2\text{-O}_2$  电池测试中以该催化剂为阴极的电池在电池电压为  $0.34 \text{ V}$  时,电池的电流密度达到了  $0.1 \text{ A} \cdot \text{cm}^{-2}$ ,为相同条件下以商业铂碳催化剂为阴极电池性能的40%,如图2A。尽管相较于目前研究最多的 M/N/C ( $\text{M} = \text{Fe}, \text{Co}$ ) 催化剂,该催化剂的催化活性还有一定的差距,然而该催化剂的稳定性非常优秀。在  $210 \text{ h}$  的电池测试过程中,电池的电压仅下降了

8%,且重复启动时电池的电压能够完全恢复初始值,更重要的是该催化剂在有毒化气体( $\text{SO}_2$ )存在的情况下仍然能够保持电池性能基本不变(图2B)。

针对包覆型非贵金属氧还原催化剂活性仍较低的现状,研究人员通过强化包覆过渡金属与外层碳壳的作用,采用改变包覆过渡金属结构的方法有效地提升了该类催化剂在酸性条件下氧还原的性能。2014年,Hu等<sup>[32]</sup>报导了石墨碳层包覆碳化铁粒子空心球的氧还原催化剂( $\text{Fe}_3\text{C/C}$ )。通过温度优化得到了性能较好的催化剂,其在氧气饱和的  $0.1 \text{ mol} \cdot \text{L}^{-1} \text{HClO}_4$  中催化剂的起始电位达到了  $0.9 \text{ V}$ ,半波电位达到了  $0.73 \text{ V}$ ,同时该催化剂拥有较高的质量比活性,在  $0.8 \text{ V}$  的条件下达到了  $0.5 \text{ A} \cdot \text{g}^{-1}$ 。该催化剂的性能达到了目前报导的 M/N/C ( $\text{M} = \text{Fe}, \text{Co}$ ) 催化剂的水平(图3)。

2015年,Zhu等<sup>[34]</sup>用廉价的二氰二胺、氧化炭黑和氯化铁为前驱体制备了一系列的氮掺杂碳纳米管包覆碳化铁粒子/碳复合催化剂( $\text{Fe}_3\text{C/NCNTs/C}$ )。得益于催化剂交联的碳纳米管/碳组成和薄壁碳管包覆碳化铁粒子的结构,该催化剂在酸性条件下表现出优异的氧还原性能,起始还原电位和半波电位分别达到了  $0.928 \text{ V}$  和  $0.785 \text{ V}$ ,超过了报导的大多数非贵金属氧还原催化剂。同时该催化剂具有超低的双氧水产率,在整个测试电位区间内其双氧水产率低于1%。Xiao等<sup>[33]</sup>报导了以萘二胺、氯化铁为前驱体通过聚合热解的方法制备

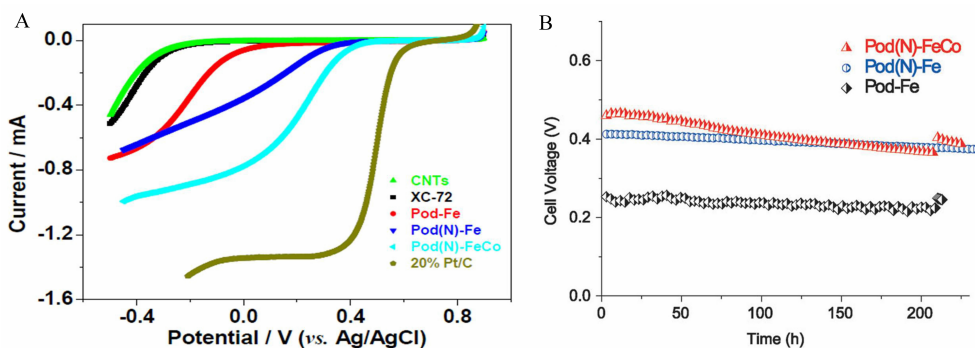


图2 A.  $0.1 \text{ mol} \cdot \text{L}^{-1} \text{H}_2\text{SO}_4$  中、 $25^\circ\text{C}$  条件下通过旋转圆盘电极测试得到的 Pod-Fe、Pod(N)-Fe、Pod(N)-FeCo 以及对比样 CNTs、XC-72 和商业 Pt/C 催化剂性能;B. 以 Pod-Fe、Pod(N)-Fe、Pod(N)-FeCo 为阴极催化剂组装的氢-氧燃料电池分别在其稳态电流  $0.1$ 、 $0.5$  和  $0.5 \text{ A}$  条件下测试电池稳定性(Pod-Fe 催化剂在  $70^\circ\text{C}$ 、 $2.0 \times 10^5 \text{ Pa}$  条件下测试)<sup>[36]</sup>

Fig. 2 A. ORR activities of Pod-Fe, Pod(N)-Fe, Pod(N)-FeCo in comparison to CNTs, XC-72 and commercial 20% Pt/C based on the rotating disk electrode (RDE) tests in  $0.1 \text{ mol} \cdot \text{L}^{-1} \text{H}_2\text{SO}_4$  solution at  $25^\circ\text{C}$ ; B.  $\text{H}_2\text{-O}_2$  fuel cell durability test results with the Pod-Fe, Pod(N)-Fe, Pod(N)-FeCo cathodes at a steady current of  $0.1$ ,  $0.5$ , and  $0.5 \text{ A}$ , respectively (Pod-Fe at  $70^\circ\text{C}$  and  $2.0 \times 10^5 \text{ Pa}$ )<sup>[36]</sup>



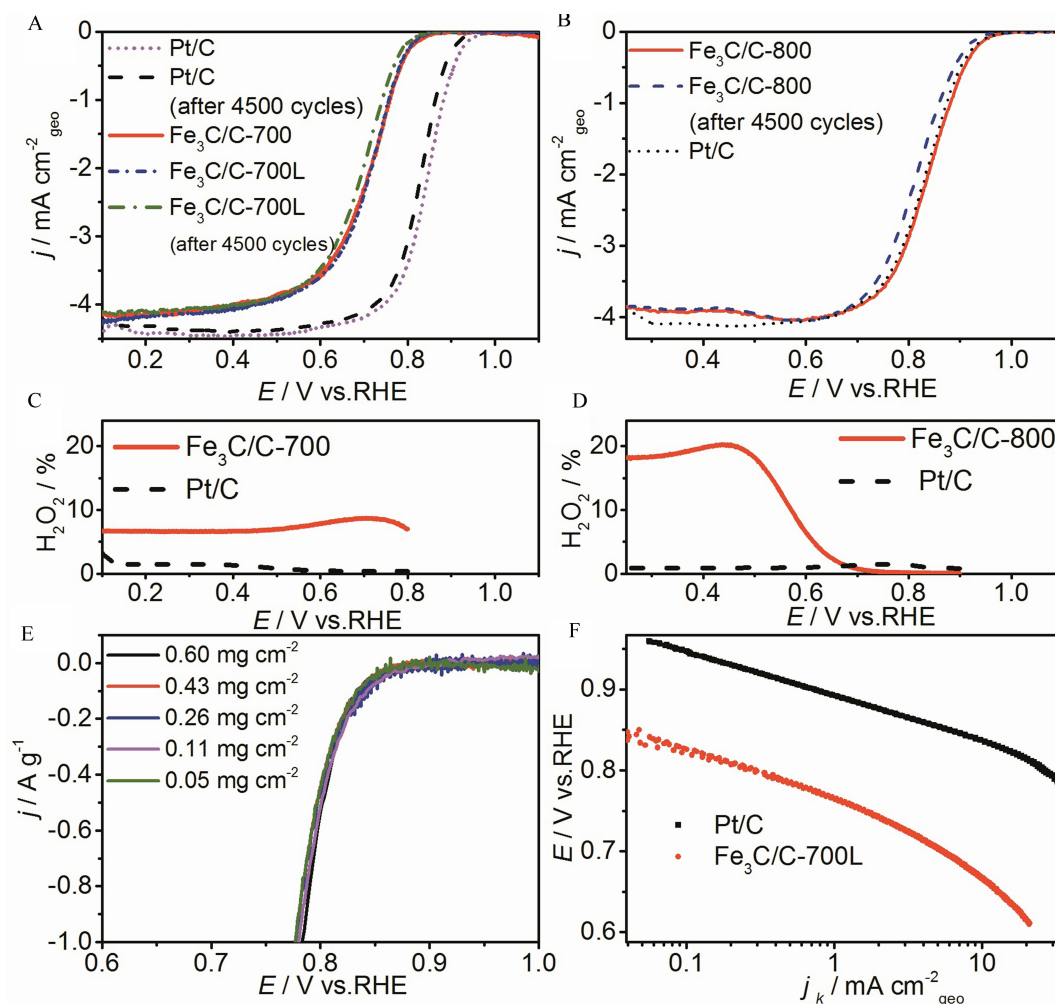


图 3 A.  $\text{Fe}_3\text{C}/\text{C}$ -700,  $\text{Fe}_3\text{C}/\text{C}$ -700L 和 Pt/C 催化剂在氧饱和和  $0.1 \text{ mol} \cdot \text{L}^{-1} \text{HClO}_4$  中 4500 周电势扫描前后的线性扫描曲线; B.  $\text{Fe}_3\text{C}/\text{C}$ -800 和 Pt/C 催化剂在氧饱和和  $0.1 \text{ mol} \cdot \text{L}^{-1} \text{KOH}$  中 4500 周电势扫描前后的线性扫描曲线; C.  $\text{Fe}_3\text{C}/\text{C}$ -700 和 Pt/C 催化剂在  $0.1 \text{ mol} \cdot \text{L}^{-1} \text{HClO}_4$  中双氧水的产率; D.  $\text{Fe}_3\text{C}/\text{C}$ -800 和 Pt/C 催化剂在  $0.1 \text{ mol} \cdot \text{L}^{-1} \text{KOH}$  双氧水产率; E.  $0.1 \text{ mol} \cdot \text{L}^{-1} \text{HClO}_4$  中  $\text{Fe}_3\text{C}/\text{C}$ -700 催化剂电极载量与催化性能的关系; F.  $\text{Fe}_3\text{C}/\text{C}$ -800 和 Pt/C 催化剂的 Tafel 曲线 ( $\text{Fe}_3\text{C}/\text{C}$ -700 和 Pt/C 的电极载量分别为  $0.25 \text{ mg} \cdot \text{cm}^{-2}$  和  $50 \mu\text{g}_\text{Pt} \cdot \text{cm}^{-2}$ )<sup>[32]</sup>

Fig. 3 A. Linear sweep voltammograms (LSVs) of  $\text{Fe}_3\text{C}/\text{C}$ -700,  $\text{Fe}_3\text{C}/\text{C}$ -700L and Pt/C (20% Pt on Vulcan XC-72, Johnson Matthey) at  $900 \text{ r} \cdot \text{min}^{-1}$  in  $\text{O}_2$ -saturated  $0.1 \text{ mol} \cdot \text{L}^{-1} \text{HClO}_4$  before and after 4500 potential cycles. Potential cycling was carried out between 0.6 and 1.0 V in  $\text{N}_2$ -saturated  $0.1 \text{ mol} \cdot \text{L}^{-1} \text{HClO}_4$ ; B. LSVs of  $\text{Fe}_3\text{C}/\text{C}$ -800 and Pt/C at  $900 \text{ r} \cdot \text{min}^{-1}$  in  $\text{O}_2$ -saturated  $0.1 \text{ mol} \cdot \text{L}^{-1} \text{KOH}$  before and after 4500 potential cycles. Potential cycling was carried out between 0.6 and 1.0 V in  $\text{N}_2$ -saturated  $0.1 \text{ mol} \cdot \text{L}^{-1} \text{KOH}$ ; C. Hydrogen peroxide yields of the  $\text{Fe}_3\text{C}/\text{C}$ -700 and Pt/C catalysts for the ORR in  $0.1 \text{ mol} \cdot \text{L}^{-1} \text{HClO}_4$ ; D. Hydrogen peroxide yields of the  $\text{Fe}_3\text{C}/\text{C}$ -800 and Pt/C catalysts for the ORR in  $0.1 \text{ mol} \cdot \text{L}^{-1} \text{KOH}$ ; E. Mass-specific LSVs of  $\text{Fe}_3\text{C}/\text{C}$ -700 with different catalyst loadings on RDE tests at  $900 \text{ r} \cdot \text{min}^{-1}$  in  $\text{O}_2$ -saturated  $0.1 \text{ mol} \cdot \text{L}^{-1} \text{HClO}_4$ ; F. Tafel plots obtained from the RDE measurements on  $\text{Fe}_3\text{C}/\text{C}$ -700 and Pt/C at  $900 \text{ r} \cdot \text{min}^{-1}$ . The catalyst loadings were  $0.6 \text{ mg} \cdot \text{cm}^{-2}$  for  $\text{Fe}_3\text{C}/\text{C}$  catalyst and  $0.25 \text{ mg} \cdot \text{cm}^{-2}$  ( $50 \mu\text{g}_\text{Pt} \cdot \text{cm}^{-2}$ ) for Pt/C catalyst. The scan rate was  $10 \text{ mV} \cdot \text{s}^{-1}$ .<sup>[32]</sup>

了具有大孔/介孔结构的石墨碳层包覆碳化铁纳米粒子催化剂, 催化剂的三维分级孔结构和石墨碳层包覆碳化铁纳米粒子的协同作用使催化剂的活性得到了显著提升, 其氧气的起始还原电位达到了  $0.92 \text{ V}$ , 半波电位为  $0.77 \text{ V}$ , 如图 4 所示. 其中,

催化剂结构中的大孔/介孔三维结构在确保了氧还原过程中电子和反应物传输速率的同时提高了催化剂的活性位点密度, 提升了催化剂的催化效率. 以上研究表明, 碳层包覆碳化铁粒子的独特结构可以提高催化剂活性位点的催化活性.



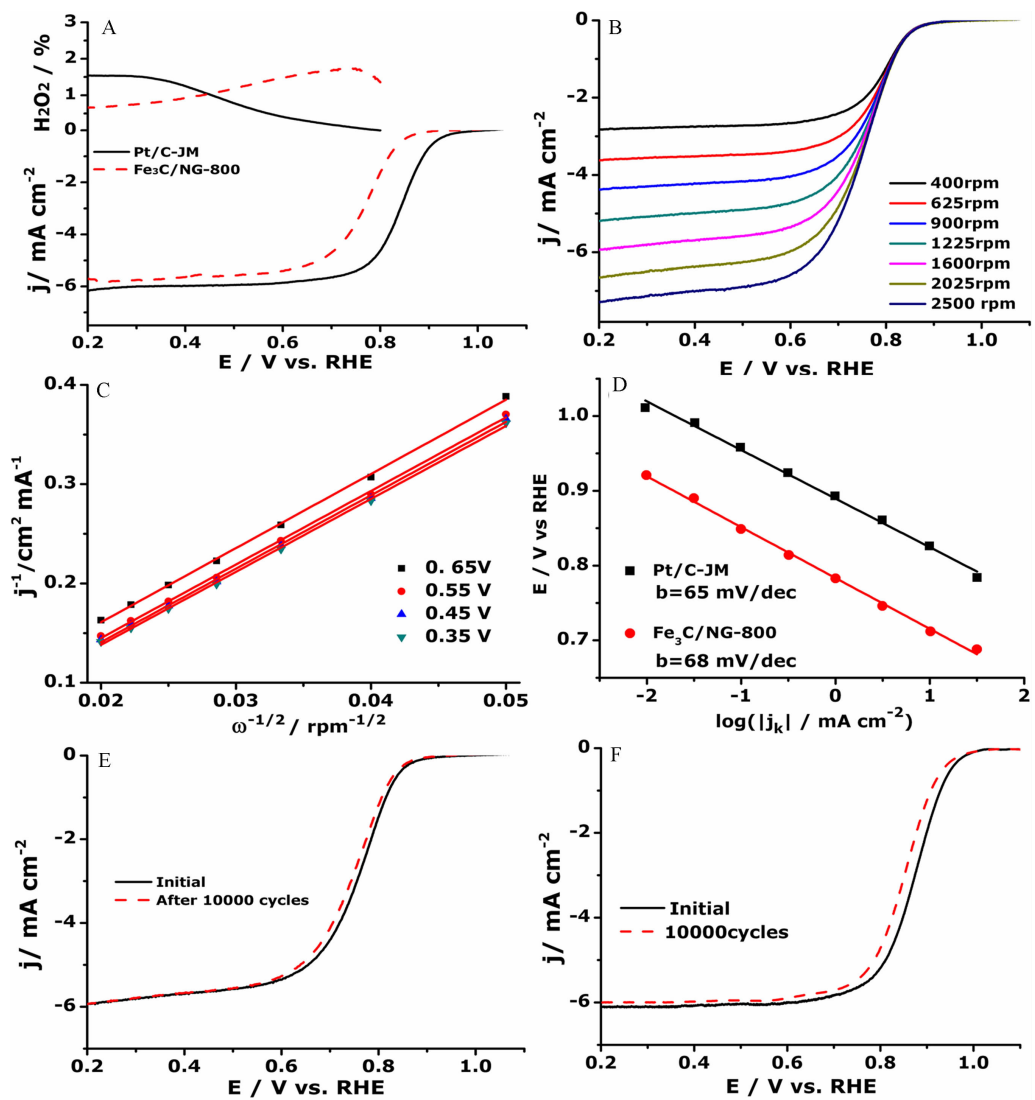


图 4 A. 0.1 mol·L<sup>-1</sup> HClO<sub>4</sub> 氧饱和条件下测得的 Fe<sub>3</sub>C/NG-800 和 Pt/C-JM 催化剂的极化曲线和双氧水产率,测试条件为: 扫速 5 mV·s<sup>-1</sup>,转速 1600 r·min<sup>-1</sup>;B. Fe<sub>3</sub>C/NG-800 催化剂在不同转速条件下测得的极化曲线,扫速为 5 mV·s<sup>-1</sup>;C. 根据不同转速数据得到的 Koutecky-Levich (K-L) 曲线;D. Fe<sub>3</sub>C/NG-800 和 Pt/C-JM 催化剂的 Tafel 曲线;E. Fe<sub>3</sub>C/NG-800 催化剂稳定性测试前后的极化曲线;F. 商业 Pt/C 催化剂稳定性测试前后的极化曲线<sup>[33]</sup>

Fig. 4 A. RDE polarization curves and hydrogen peroxides yields of Fe<sub>3</sub>C/NG-800 and Pt/C-JM in O<sub>2</sub>-saturated 0.1 mol·L<sup>-1</sup> HClO<sub>4</sub> with a scan rate of 5 mV·s<sup>-1</sup> and a rotation speed of 1600 r·min<sup>-1</sup>; B. Linear sweep voltammograms for oxygen reduction on the Fe<sub>3</sub>C/NG-800 catalyst in O<sub>2</sub>-saturated 0.1 mol·L<sup>-1</sup> HClO<sub>4</sub> at various rotation speeds with a scan rate of 5 mV·s<sup>-1</sup>; C. Corresponding Koutecky-Levich (K-L) plots; D. Tafel plots for Fe<sub>3</sub>C/NG-800 and Pt/C-JM extracted from the data in panel A; ORR polarization plots of (E) Fe<sub>3</sub>C/NG-800 and (F) Pt/C before and after 10000 potential cycles in O<sub>2</sub>-saturated 0.1 mol·L<sup>-1</sup> HClO<sub>4</sub>. The potential was cycled between 0.6 and 1.2 V at a rate of 50 mV·s<sup>-1</sup>. The loadings of catalysts were 0.4 mg·cm<sup>-2</sup> for the Fe<sub>3</sub>C/NG catalysts and 20 μg<sub>Pt</sub>·cm<sup>-2</sup> for the commercial Pt/C<sup>[33]</sup>

尽管在酸性条件下这些催化剂的活性与商业铂碳催化剂还有一定差距,然而得益于该类催化剂抗磷酸、甲醇的毒化能力和优异的稳定性,该类催化剂在以 PBI 为质子交换膜的高温燃料电池和直接甲醇燃料电池中有潜在的应用. Hu 等<sup>[42]</sup>用

Fe<sub>3</sub>C/C-700 催化剂为阴极在 PBI 膜燃料电池中测试,当温度为 160 °C 时电池功率密度达到了 60 mW·cm<sup>-2</sup>. Zhu 和 Xiao 等<sup>[34]</sup>分别以 Fe<sub>3</sub>C/NCNTs/C 和 Fe<sub>3</sub>C/NG-800 催化剂替代铂碳催化剂组装了直接甲醇燃料电池测试,电池的开路电压与铂碳催化

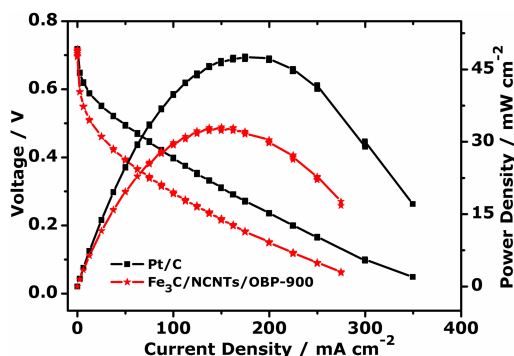


图5 以 Pt/C 或  $\text{Fe}_3\text{C}/\text{NCNTs}/\text{OBP-900}$  催化剂为阴极组装直接甲醇燃料电池在  $60\text{ }^\circ\text{C}$  条件下的极化曲线, 阴极贵金属 Pt 或  $\text{Fe}_3\text{C}/\text{NCNTs}/\text{OBP-900}$  催化剂载量均为  $3\text{ mg}\cdot\text{cm}^{-2}$ , 阳极 为 PtRu 载量为  $2\text{ mg}_{\text{metal}}\cdot\text{cm}^{-2}$ , 甲醇流速为  $5\text{ mL}\cdot\text{min}^{-1}$ , 氧气流速为  $100\text{ mL}\cdot\text{min}^{-1}$ [34]

Fig. 5 Performance of the acidic direct methanol fuel cell at  $60\text{ }^\circ\text{C}$  with Pt/C (20%,  $3\text{ mg}_{\text{Pt}}\cdot\text{cm}^{-2}$ ) or  $\text{Fe}_3\text{C}/\text{NCNTs}/\text{OBP-900}$  ( $3\text{ mg}\cdot\text{cm}^{-2}$ ) as the cathode catalysts. The anode catalyst was PtRu/C (30%,  $2\text{ mg}_{\text{metal}}\cdot\text{cm}^{-2}$ ) with  $2\text{ mol}\cdot\text{L}^{-1}$   $\text{CH}_3\text{OH}$  supplied at a flow rate of  $5\text{ mL}\cdot\text{min}^{-1}$ . Dry oxygen was supplied to the cathode at a flow rate of  $100\text{ mL}\cdot\text{min}^{-1}$ [34].

剂为阴极的电池相近,同时单电池的最大功率密度分别达到了  $31.2$  和  $22\text{ mW}\cdot\text{cm}^{-2}$ , 为相同条件下铂碳催化剂的  $69.3\%$ 和  $48.9\%$ , 且电池的稳定性得到了显著的提高(图 5). 这表明,尽管所采用的非贵金属催化剂的活性与商业铂碳催化剂有一定的差距,但在直接甲醇燃料电池中该差距被明显缩小.

## 2.2 碱性条件下包覆型非贵金属氧还原催化剂性能

对碱性条件下包覆型非贵金属氧还原催化剂的研究较为广泛, 表 1 列举了目前报导的用于碱性条件下氧还原的包覆型非贵金属催化剂. 可以看出, 在碱性条件下包覆型非贵金属催化剂的种类更为丰富且均表现出较为优异的催化氧还原性能. Yang 等[43]采用软模板法合成了氮掺杂碳纳米管包覆  $\text{Fe}_3\text{C}$  粒子催化剂, 在碱性电解质中表现出较高的氧还原活性、稳定性和抗甲醇毒化能力. Li 等[44]利用金属有机配偶物骨架结构同时作为模板材料和铁源合成了氮掺杂碳  $\text{Fe}/\text{Fe}_3\text{C}$  混合相的氧还原催化剂, 催化剂为石墨烯和碳纳米管的复合相, 在碱性条件下表现出了优异的氧还原性能. 冯

表 1 碱性条件下包覆型非贵金属氧还原催化剂性能总结

Tab. 1 Summary of ORR activities for different non-precious metal catalysts in alkaline media

Catalysts	Electrolyte	Activity		Reference
		Onset/V	$E_{1/2}/\text{V}$	
N-doped $\text{Fe}/\text{Fe}_3\text{C}@/\text{RGO}$	$0.1\text{ mol}\cdot\text{L}^{-1}\text{ KOH}$	1.0	0.93	[45]
N-doped $\text{Fe}/\text{Fe}_3\text{C}@/\text{C}$	$0.1\text{ mol}\cdot\text{L}^{-1}\text{ KOH}$	0.91	0.83	[45]
$\text{Fe}_3\text{C}/\text{C-700}$	$0.1\text{ mol}\cdot\text{L}^{-1}\text{ KOH}$	1.05	0.83	[32]
$\text{Fe}_3\text{C}/\text{NG-800}$	$0.1\text{ mol}\cdot\text{L}^{-1}\text{ KOH}$	1.03	0.86	[33]
$\text{Fe}_3\text{C}/\text{NCNTs}/\text{OBP-900}$	$0.1\text{ mol}\cdot\text{L}^{-1}\text{ KOH}$	1.05	0.92	[34]
$\text{Fe}/\text{Fe}_3\text{C}@/\text{NC}$	$0.1\text{ mol}\cdot\text{L}^{-1}\text{ KOH}$	0.766	—	[44]
$\text{Fe}/\text{Fe}_3\text{C}@/\text{NGL-NCNT}$	$0.1\text{ mol}\cdot\text{L}^{-1}\text{ KOH}$	0.996	—	[44]
$\text{Co}_x\text{P-CNTs-1000}$	$0.1\text{ mol}\cdot\text{L}^{-1}\text{ KOH}$	0.836	—	[46]
$\text{M}_3\text{C-GNRs}$	$0.1\text{ mol}\cdot\text{L}^{-1}\text{ KOH}$	0.8	—	[38]
N-Fe-CNT/CNP	$0.1\text{ mol}\cdot\text{L}^{-1}\text{ KOH}$	1.07	0.87	[47]
$\text{Fe}_3\text{C}@/\text{NCNTs-800}$	$0.1\text{ mol}\cdot\text{L}^{-1}\text{ KOH}$	1.07	0.82	[48]
$\text{Fe}@/\text{N-C}/\text{SiC}@/\text{N-C}$	$0.1\text{ mol}\cdot\text{L}^{-1}\text{ KOH}$	0.88	—	[49]
$\text{Fe}_3\text{C}@/\text{NCNF-900}$	$0.1\text{ mol}\cdot\text{L}^{-1}\text{ KOH}$	0.94	—	[50]
N-HG	$0.1\text{ mol}\cdot\text{L}^{-1}\text{ KOH}$	0.92	—	[51]
$\text{Fe}/\text{N-CNTs}$	$0.1\text{ mol}\cdot\text{L}^{-1}\text{ KOH}$	0.96	—	[52]
$\text{Co}/\text{N-CNT}$	$0.1\text{ mol}\cdot\text{L}^{-1}\text{ KOH}$	0.94	0.84	[52]

新亮和 Müllen 课题组<sup>[37]</sup>报导了具有三维结构的氮掺杂石墨稀包覆  $\text{Fe}_3\text{O}_4$  粒子催化剂,在碱性条件下具有很高的氧还原活性、选择性和稳定性,这主要得益于催化剂的大比表面积、三维孔结构和包覆  $\text{Fe}_3\text{O}_4$  的结构. Zelenay 课题组<sup>[47]</sup>将单氰胺、醋酸亚铁和氧化碳黑混合后热解,热解产物在  $0.5 \text{ mol} \cdot \text{L}^{-1} \text{H}_2\text{SO}_4$  中除去不稳定相,而后再热解,得到氮掺杂碳纳米管包覆含铁粒子的非贵金属催化剂.该催化剂具有很高的氧还原活性和稳定性,在氧饱和的  $0.1 \text{ mol} \cdot \text{L}^{-1} \text{NaOH}$  中其半波电位达到了  $0.93 \text{ V}$ ,为目前文献报导的性能最好的非贵金属氧还原催化剂(图 6).

### 3 包覆型非贵金属氧还原催化剂机理研究

对包覆型非贵金属氧还原催化剂催化机理的

研究主要集中在包覆的过渡金属对外层碳壳的电子修饰方面.例如,包信和等<sup>[36,41]</sup>通过原位近边吸收 X-射线和理论计算对碳氮包覆铁纳米粒子催化剂的活性位点进行了深入的研究.研究表明,包覆 Fe 不直接参与氧还原过程当中,在该类型催化剂中活性位为包覆金属颗粒的氮碳组分.密度泛函计算表明,包覆的铁纳米粒子显著地改变外层碳原子接近费米能及附近低态密度区域的电子结构.深入分析表明,包覆的 Fe 纳米粒子将电子转移到与其临近的碳原子上,提高了碳原子的费米能级,在表层碳上诱导形成局部偶极作用.这些作用使得表层碳原子的局部功函降低并提高了其反应性,如图 7 所示.

Zhu 等<sup>[34]</sup>对氮掺杂碳包覆  $\text{Fe}_3\text{C}$  粒子催化剂的计算也得出了类似的结论,并通过对催化剂表面

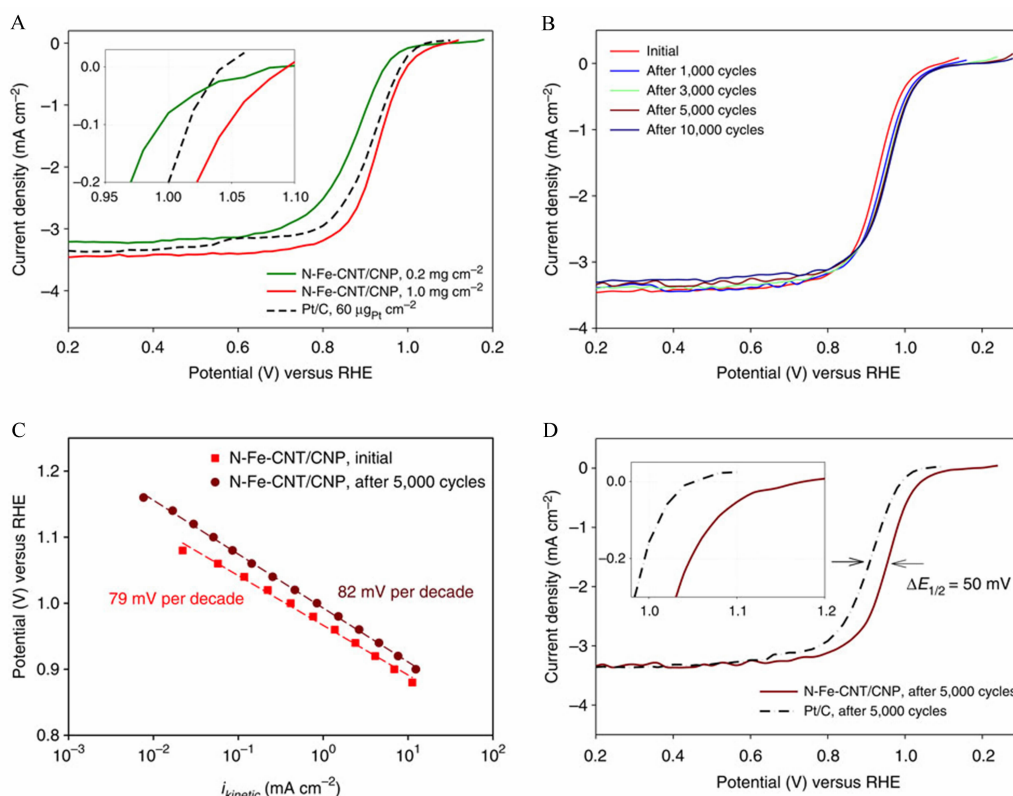
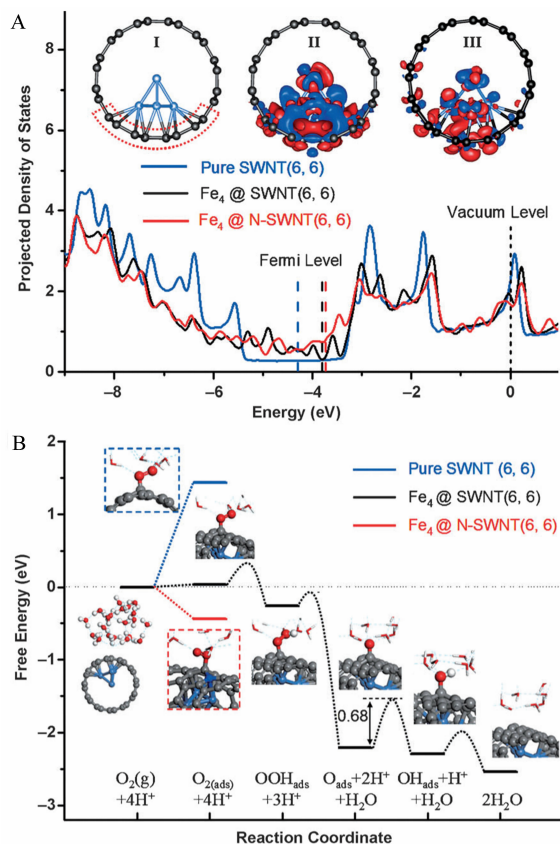


图 6 A. N-Fe-CNT/CNP 催化剂稳定性测试前在氧饱和的  $0.1 \text{ mol} \cdot \text{L}^{-1} \text{NaOH}$  溶液中测得的极化曲线;B. N-Fe-CNT/CNP 催化剂经过不同周数的稳定性测试后的极化曲线;C. 催化剂 5000 周稳定性测试前后的 Tafel 曲线;D. 5000 周稳定性测试后催化剂在氧饱和电解液中的极化曲线<sup>[47]</sup>

Fig. 6 A. RDE polarization plots before cycling durability test; B. RDE polarization plots measured during cycling durability test in  $\text{O}_2$ -saturated  $0.1 \text{ mol} \cdot \text{L}^{-1} \text{NaOH}$  (cycling in the potential range  $0.6 \sim 1.0 \text{ V}$  at  $50 \text{ mV} \cdot \text{s}^{-1}$ ; N-Fe-CNT/CNP loading  $1.0 \text{ mg} \cdot \text{cm}^{-2}$ ); C. Tafel plots for the N-Fe-CNT/CNP catalyst before and after 5000 cycles in an  $\text{O}_2$ -saturated electrolyte (Tafel slope calculated by linear regression method in the intermediate range of current densities,  $10^{-2} \sim 10 \text{ mA} \cdot \text{cm}^{-2}$ ); D. RDE polarization plots after 5000 cycles in  $\text{O}_2$ -saturated electrolyte<sup>[47]</sup>



图 7 DFT 计算结果<sup>[36,41]</sup>

A. 在  $\text{Fe}_4@\text{SWNT}$  和  $\text{Fe}_4@\text{N-SWNT}$  中与  $\text{Fe}_4$  键和碳原子 p 轨道的局部电子态密度; B. 在实验条件下氧气在  $\text{Fe}_4@\text{SWNT}$  上还原的自由能曲线

Fig. 7 Results of DFT calculations<sup>[36,41]</sup>

A. Projected DOS of the p orbitals of C atoms bonded to  $\text{Fe}_4$  in  $\text{Fe}_4@\text{SWNT}$  and  $\text{Fe}_4@\text{N-SWNT}$  compared with that in pure SWNT. The vacuum level is aligned at 0 eV. Inserted plot I and plot II show the optimized structure of  $\text{Fe}_4@\text{SWNT}$  and its difference in charge density, and Figures S18 and plot III correspond to that of  $\text{Fe}_4@\text{N-SWNT}$ . The red and blue regions in plot II and III indicate a charge increase and decrease, respectively; B. Free-energy diagram of ORR on  $\text{Fe}_4@\text{SWNT}$  in water (black line) under experimental conditions (onset potential = 0.6 V vs. normal hydrogen electrode (NHE), pH = 0)

氮元素组份与催化剂催化性能的定量分析表明氮元素并不直接参与到氧还原反应中(图 8). 与铁的作用相类似, 氮元素的引入能进一步提高相关区域碳原子近费米能级附近的态密度, 降低掺杂区域碳原子的局部功函, 从而更进一步地提高了催化剂的氧还原性能. Hu 和 Chen 等<sup>[32, 46]</sup>在实验上对

包覆型催化剂活性位点进行了研究, 他们先采用球磨破坏包覆过渡金属的碳层, 然后酸洗除去过渡金属相. 结果显示, 除去过渡金属相的催化剂的催化性能降低到和普通碳黑相接近, 进一步采用无氮源的合成方法合成纯碳层包覆  $\text{Fe}_3\text{C}$  的催化剂则未表现出明显的氧还原催化性能, 如图 9 所示. 以上结果表明, 在该类催化剂中包覆的过渡金属与氮组分都对提升催化剂活性起着不可或缺的作用.

## 4 总结与展望

包覆型过渡金属氧还原催化剂作为一类新兴的贵金属替代催化剂, 其优异的活性、稳定性将在解决燃料电池、金属-空气电池等能源转换装置成本问题以及促进其商业化等方面起到重要作用. 同时, 其独特的包覆结构为研究非贵金属氧还原催化剂的活性位点提供了一个优良的平台, 对认识非贵金属氧还原催化剂的催化机理、催化位点有着重要意义. 未来对该类催化剂的研究方向可着眼于:

1) 在催化剂的制备方面, 开发更加简单、可批量合成的方法, 减少催化剂合成方面的不可控因素. 对催化剂的电池性能做更深入的研究, 在全电池/电堆系统中对催化剂性能进行评价.

2) 深入对催化剂活性位点的研究, 包覆过渡金属对外层的石墨化氮碳层的作用机制、氧气在该类催化剂上的反应机理及影响因素进行深入研究

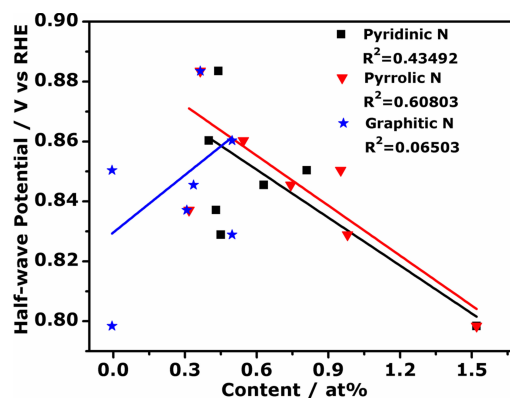


图 8 不同热处理温度、时间得到的  $\text{Fe}_3\text{C}/\text{NCNTs}/\text{OBP}$  催化剂中吡啉氮、吡咯氮和石墨氮与氧还原半波电位的线性关系<sup>[34]</sup>

Fig. 8 Atomic percentages of pyridinic N, pyrrolic N and graphitic N versus half-wave potentials of  $\text{Fe}_3\text{C}/\text{NCNTs}/\text{OBP}$  catalysts heat-treated at various temperatures and time<sup>[34]</sup>

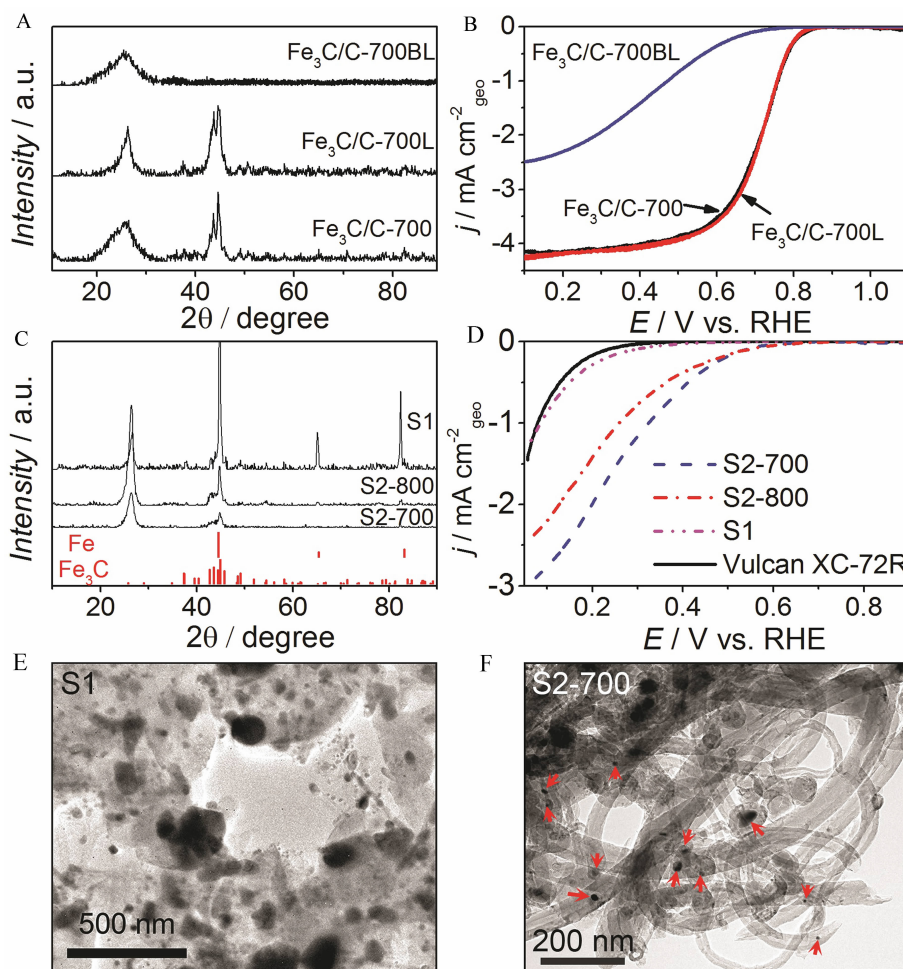


图9 A.  $\text{Fe}_3\text{C}/\text{C}-700$ 、 $\text{Fe}_3\text{C}/\text{C}-700\text{L}$  和  $\text{Fe}_3\text{C}/\text{C}-700\text{BL}$  催化剂的 XRD 图谱; B. 经过球磨酸洗除去包覆的  $\text{Fe}_3\text{C}$  组份后催化剂在  $0.1 \text{ mol} \cdot \text{L}^{-1} \text{HClO}_4$  中的氧还原线性扫描曲线; C. 前驱体中不引入氮源合成的催化剂的 XRD 谱图; D. Vulcan XC-72R、S1、S2-700 和 S2-800 在  $0.1 \text{ mol} \cdot \text{L}^{-1} \text{HClO}_4$  中的氧还原线性扫描曲线; E-F. 前驱体中不引入氮源合成的催化剂的透射电镜照片<sup>[32,46]</sup>

Fig. 9 A. XRD patterns of  $\text{Fe}_3\text{C}/\text{C}-700$ ,  $\text{Fe}_3\text{C}/\text{C}-700\text{L}$ , and  $\text{Fe}_3\text{C}/\text{C}-700\text{BL}$ ; B. The corresponding ORR LSVs at  $900 \text{ r} \cdot \text{min}^{-1}$  in  $\text{O}_2$ -saturated  $0.1 \text{ mol} \cdot \text{L}^{-1} \text{HClO}_4$ ; the scan rate was  $10 \text{ mV} \cdot \text{s}^{-1}$ ; C. XRD patterns of samples S1, S2-700, and S2-800 (see the Supporting Information for experimental details); D. ORR LSVs of Vulcan XC-72R, S1, S2-700, and S2-800 at  $900 \text{ r} \cdot \text{min}^{-1}$  in  $\text{O}_2$ -saturated  $0.1 \text{ mol} \cdot \text{L}^{-1} \text{HClO}_4$ . The catalyst loadings were  $0.6 \text{ mg} \cdot \text{cm}^{-2}$  for all the electrodes; E-F. TEM images of the samples S1 and S2-700. The arrows indicate the encapsulated  $\text{Fe}_3\text{C}$  particles.<sup>[32,46]</sup>

究,以指导实验,优化合成条件.

以上问题的解决必将对加快实现非贵金属氧还原催化剂的理性设计和可控合成,对推动燃料电池等的商业化进程起重要的作用.

## 参考文献 (References):

- [1] Jasinski R. A new fuel cell cathode catalyst[J]. *Nature*, 1964, 201(4925): 1212-1213.
- [2] Randin J P. Interpretation of the relative electrochemical activity of various metal phthalocyanines for the oxygen reduction reaction[J]. *Electrochimica Acta*, 1974, 19(2): 83-85.
- [3] Collman J P, Denisevich P, Konai Y, et al. Electrode catalysis of the four-electron reduction of oxygen to water by di cobalt face-to-face porphyrins[J]. *Journal of the American Chemical Society*, 1980, 102(19): 6027-6036.
- [4] Forshey P A, Kuwana T. Electrochemistry of oxygen reduction. 4. Oxygen to water conversion by iron(II)(tetrakis (N-methyl-4-pyridyl) porphyrin) via hydrogen peroxide[J]. *Inorganic Chemistry*, 1983, 22(5): 699-707.
- [5] Shigehara K, Anson F C. Electrocatalytic activity of three

- iron porphyrins in the reduction of dioxygen and hydrogen peroxide at graphite cathodes[J]. *The Journal of Physical Chemistry*, 1982, 86(14): 2776-2783.
- [6] Van Veen J, Colijn H. Oxygen reduction on transition-metal porphyrins in acid electrolyte II. Stability[J]. *Berichte der Bunsengesellschaft für physikalische Chemie*, 1981, 85(9): 700-704.
- [7] Chan R J, Su Y O, Kuwana T. Electrocatalysis of oxygen reduction. 5. Oxygen to hydrogen peroxide conversion by cobalt(II) tetrakis(N-methyl-4-pyridyl) porphyrin[J]. *Inorganic Chemistry*, 1985, 24(23): 3777-3784.
- [8] Jones R D, Summerville D A, Basolo F. Manganese(II) porphyrin oxygen carriers. Equilibrium constants for the reaction of dioxygen with para-substituted meso-tetraphenylporphyrinatomanganese (II) complexes [J]. *Journal of the American Chemical Society*, 1978, 100(14): 4416-4424.
- [9] Van Veen J, Van Baar J, Kroese C, et al. Oxygen reduction on transition-metal porphyrins in acid electrolyte I. Activity[J]. *Berichte der Bunsengesellschaft für physikalische Chemie*, 1981, 85(9): 693-700.
- [10] Durand Jr R R, Bencosme C S, Collman J P, et al. Mechanistic aspects of the catalytic reduction of dioxygen by cofacial metalloporphyrins[J]. *Journal of the American Chemical Society*, 1983, 105(9): 2710-2718.
- [11] Collman J P, Gagne R R, Reed C, et al. Picket fence porphyrins. Synthetic models for oxygen binding hemoproteins[J]. *Journal of the American Chemical Society*, 1975, 97(6): 1427-1439.
- [12] Collman J P, Kim K. Electrocatalytic four-electron reduction of dioxygen by iridium porphyrins adsorbed on graphite[J]. *Journal of the American Chemical Society*, 1986, 108(24): 7847-7849.
- [13] Vasudevan P, Mann N, Tyagi S. Transition metal complexes of porphyrins and phthalocyanines as electrocatalysts for dioxygen reduction[J]. *Transition Metal Chemistry*, 1990, 15(2): 81-90.
- [14] Van den Brink F, Barendrecht E, Visscher W. The cathodic reduction of oxygen: A review with emphasis on macrocyclic organic metal complexes as electrocatalysts [J]. *Recueil des Travaux Chimiques des Pays-Bas*, 1980, 99(9): 253-262.
- [15] van Wingerden B, van Veen J R, Mensch C T. An extended X-ray absorption fine structure study of heat-treated cobalt porphyrin catalysts supported on active carbon [J]. *Journal of the Chemical Society, Faraday Transactions 1: Physical Chemistry in Condensed Phases*, 1988, 84(1): 65-74.
- [16] Keda O, Fukuda H, Tamura H. The effect of heat treatment on group VIII B porphyrins as electrocatalysts in the cathodic reduction of oxygen[J]. *Journal of the Chemical Society, Faraday Transactions 1: Physical Chemistry in Condensed Phases*. 1986, 82(5): 1561-1573.
- [17] Gupta S, Tryk D, Bae I, et al. Heat-treated polyacrylonitrile-based catalysts for oxygen electroreduction[J]. *Journal of Applied Electrochemistry*, 1989, 19(1): 19-27.
- [18] Savy M, Coowar F, Riga J, et al. Investigation of O<sub>2</sub> reduction in alkaline media on macrocyclic chelates impregnated on different supports: Influence of the heat treatment on stability and activity[J]. *Journal of Applied Electrochemistry*, 1990, 20(2): 260-268.
- [19] Lefèvre M, Proietti E, Jaouen F, et al. Iron-based catalysts with improved oxygen reduction activity in polymer electrolyte fuel cells[J]. *science*, 2009, 324(5923): 71-74.
- [20] Jaouen F, Proietti E, Lefèvre M, et al. Recent advances in non-precious metal catalysis for oxygen-reduction reaction in polymer electrolyte fuel cells[J]. *Energy & Environmental Science*, 2011, 4(1): 114-130.
- [21] Jaouen F, Herranz J, Lefevre M, et al. Cross-laboratory experimental study of non-noble-metal electrocatalysts for the oxygen reduction reaction[J]. *ACS Applied Materials & Interfaces*, 2009, 1(8): 1623-1639.
- [22] Yang S B, Feng X L, Wang X C, et al. Graphene-based carbon nitride nanosheets as efficient metal-free electrocatalysts for oxygen reduction reactions[J]. *Angewandte Chemie International Edition*, 2011, 50(23): 5339-5343.
- [23] Lefèvre M, Dodelet J, Bertrand P. Molecular oxygen reduction in PEM fuel cells: Evidence for the simultaneous presence of two active sites in Fe-based catalysts[J]. *The Journal of Physical Chemistry B*, 2002, 106(34): 8705-8713.
- [24] Li W M, Wu J, Higgins D C, et al. Determination of iron active sites in pyrolyzed iron-based catalysts for the oxygen reduction reaction[J]. *ACS Catalysis*, 2012, 2(12): 2761-2768.
- [25] Qu L T, Liu Y, Baek J B, et al. Nitrogen-doped graphene as efficient metal-free electrocatalyst for oxygen reduction in fuel cells[J]. *ACS Nano*, 2010, 4(3): 1321-1326.
- [26] Yang L J, Jiang S J, Zhao Y, et al. Boron-doped carbon nanotubes as metal-free electrocatalysts for the oxygen reduction reaction[J]. *Angewandte Chemie-International Edition*, 2011, 50(31): 7132-7135.
- [27] Yang Z, Yao Z, Li G F, et al. Sulfur-doped graphene as an efficient metal-free cathode catalyst for oxygen reduction[J]. *ACS Nano*, 2011, 6(1): 205-211.
- [28] Yang D S, Bhattacharjya D, Inamdar S, et al. Phosphorus-



- doped ordered mesoporous carbons with different lengths as efficient metal-free electrocatalysts for oxygen reduction reaction in alkaline media[J]. *Journal of the American Chemical Society*, 2012, 134(39): 16127-16130.
- [29] Gong K P, Du F, Xia Z H, et al. Nitrogen-doped carbon nanotube arrays with high electrocatalytic activity for oxygen reduction[J]. *Science*, 2009, 323(5915): 760-764.
- [30] Wang J, Wang G X, Miao S, et al. Synthesis of Fe/Fe<sub>3</sub>C nanoparticles encapsulated in nitrogen-doped carbon with single-source molecular precursor for the oxygen reduction reaction[J]. *Carbon*, 2014, 75: 381-389.
- [31] Zhong G, Wang H, Yu H, et al. A novel carbon-encapsulated cobalt-tungsten carbide as electrocatalyst for oxygen reduction reaction in alkaline media[J]. *Fuel Cells*, 2013, 13(3): 387-391.
- [32] Hu Y, Jensen J O, Zhang W, et al. Hollow spheres of iron carbide nanoparticles encased in graphitic layers as oxygen reduction catalysts[J]. *Angewandte Chemie International Edition*, 2014, 53(14): 3675-3679.
- [33] Xiao M L, Zhu J B, Feng L G, et al. Meso/macroporous nitrogen-doped carbon architectures with iron carbide encapsulated in graphitic layers as an efficient and robust catalyst for the oxygen reduction reaction in both acidic and alkaline solutions[J]. *Advanced Materials*, 2015, 27(15): 2521-2527.
- [34] Zhu J B, Xiao M L, Liu C P, et al. Growth mechanism and active site probing of Fe<sub>3</sub>C@N-doped carbon nanotubes/C catalysts: Guidance for building highly efficient oxygen reduction electrocatalysts[J]. *Journal of Materials Chemistry A*, 2015, 3(43): 21451-21459.
- [35] Deng J, Yu L, Deng D H, et al. Highly active reduction of oxygen on a FeCo alloy catalyst encapsulated in pod-like carbon nanotubes with fewer walls[J]. *Journal of Materials Chemistry A*, 2013, 1(47): 14868-14873.
- [36] Deng D H, Yu L, Chen X Q, et al. Iron encapsulated within pod-like carbon nanotubes for oxygen reduction reaction[J]. *Angewandte Chemie International Edition*, 2013, 52(1): 371-375.
- [37] Wu Z S, Yang S, Sun Y, et al. 3D nitrogen-doped graphene aerogel-supported Fe<sub>3</sub>O<sub>4</sub> nanoparticles as efficient electrocatalysts for the oxygen reduction reaction[J]. *Journal of the American Chemical Society*, 2012, 134(22): 9082-9085.
- [38] Fan X J, Peng Z W, Ye R Q, et al. M<sub>3</sub>C (M: Fe, Co, Ni) nanocrystals encased in graphene nanoribbons: An active and stable bifunctional electrocatalyst for oxygen reduction and hydrogen evolution reactions[J]. *ACS Nano*, 2015, 9(7): 7407-7418.
- [39] Flahaut E, Agnoli F, Sloan J, et al. CCVD synthesis and characterization of cobalt-encapsulated nanoparticles[J]. *Chemistry of Materials*, 2002, 14(6): 2553-2558.
- [40] Cui X J, Ren P J, Deng D H, et al. Single layer graphene encapsulating non-precious metals as high-performance electrocatalysts for water oxidation[J]. *Energy & Environmental Science*, 2016, 9(1): 123-129.
- [41] Deng J, Ren P J, Deng D H, et al. Enhanced electron penetration through an ultrathin graphene layer for highly efficient catalysis of the hydrogen evolution reaction [J]. *Angewandte Chemie International Edition*, 2015, 54(7): 2100-2104.
- [42] Hu Y, Jensen J O, Zhang W, et al. Fe<sub>3</sub>C-based oxygen reduction catalysts: Synthesis, hollow spherical structures and applications in fuel cells[J]. *Journal of Materials Chemistry A*, 2015, 3(4): 1752-1760.
- [43] Yang W X, Liu X J, Yue X Y, et al. Bamboo-like carbon nanotube/Fe<sub>3</sub>C nanoparticle hybrids and their highly efficient catalysis for oxygen reduction[J]. *Journal of the American Chemical Society*, 2015, 137(4): 1436-1439.
- [44] Li J S, Li S L, Tang Y J, et al. Nitrogen-doped Fe/Fe<sub>3</sub>C@graphitic layer/carbon nanotube hybrids derived from MOFs: Efficient bifunctional electrocatalysts for ORR and OER[J]. *Chemical Communications*, 2015, 51(13): 2710-2713.
- [45] Hou Y, Huang T Z, Wen Z H, et al. Metal-organic framework-derived nitrogen-doped core-shell-structured porous Fe/Fe<sub>3</sub>C@C nanoboxes supported on graphene sheets for efficient oxygen reduction reactions[J]. *Advanced Energy Materials*, 2014, 4(11): No. 1400337.
- [46] Chen K Y, Huang X B, Wan C Y, et al. Efficient oxygen reduction catalysts formed of cobalt phosphide nanoparticle decorated heteroatom-doped mesoporous carbon nanotubes[J]. *Chemical Communications*, 2015, 51(37): 7891-7894.
- [47] Chung H T, Won J H, Zelenay P. Active and stable carbon nanotube/nanoparticle composite electrocatalyst for oxygen reduction[J]. *Nature Communications*, 2013, 4: No. 1922.
- [48] Zhong G Y, Wang H J, Yu H, et al. Nitrogen doped carbon nanotubes with encapsulated ferric carbide as excellent electrocatalyst for oxygen reduction reaction in acid and alkaline media[J]. *Journal of Power Sources*, 2015, 286: 495-503.
- [49] Li J Y, Wang J, Gao D F, et al. Silicon carbide-supported iron nanoparticles encapsulated in nitrogen-doped carbon for oxygen reduction reaction[J]. *Catalysis Science & Technology*, 2016, DOI: 10.1039/C5CY01539A.
- [50] Ren G Y, Lu X Y, Li Y, et al. Porous core-shell Fe<sub>3</sub>C em-

- bedded N-doped carbon nanofibers as an effective electrocatalysts for oxygen reduction reaction[J]. ACS Applied Materials & Interfaces, 2016, 8(6): 4118-4125.
- [51] Barman B K, Nanda K K. Prussian blue as a single precursor for synthesis of Fe/Fe<sub>3</sub>C encapsulated N-doped graphitic nanostructures as bi-functional catalysts[J]. Green Chemistry, 2016, 18(2): 427-432.
- [52] Liu Y Y, Jiang H L, Zhu Y H, et al. Transition metals (Fe, Co, and Ni) encapsulated in nitrogen-doped carbon nanotubes as bi-functional catalysts for oxygen electrode reactions[J]. Journal of Materials Chemistry A, 2016, 4(5): 1694-1701.

## Recent Progress in Non-Precious Metal Oxygen Reduction Reaction Catalysts with an Encapsulation Structure

XIAO Mei-ling<sup>1,2</sup>, ZHU Jian-bing<sup>1,2</sup>, LIU Chang-peng<sup>2</sup>, GE Jun-jie<sup>2</sup>, XING Wei<sup>1,2\*</sup>

(1. State Key Laboratory of Electroanalytical Chemistry, Changchun Institute of Applied Chemistry, Chinese Academy of Sciences, Changchun 130022, China; 2. Laboratory of Advanced Power Sources, Changchun Institute of Applied Chemistry, Changchun 130022, China)

**Abstract:** Platinum-based materials, the state-of-the-art catalysts for fuel cells, suffer from prohibitive costs, limited resources and insufficient durability. Accordingly, tremendous efforts were made in searching for efficient, durable and inexpensive alternatives to precious-metal electrocatalysts for the oxygen reduction reaction (ORR). Transition-metals (Fe, Co)/nitrogen co-doped hybrids, heteroatom (N, P, S, F, et al) doped carbons and composites with transition-metals encapsulated in graphitic layers are reported as the most efficient non-precious metal ORR catalysts. Among the various non-precious metal ORR catalysts, transition-metals encased in graphitic layer catalysts are a novel type of catalysts for ORR with high activity and durability, and thus, the in-depth researches are highly desirable. Here, we present the recent research progress in transition-metals encased catalysts from the aspects of synthesis, activity and catalytic mechanism, in an effort to promote the developments of these catalysts.

**Key words:** oxygen reduction reaction; transition-metals encased; non-precious metal catalysts